Optimization of a Phased-Array Transducer for Multiple Harmonic Imaging in Medical Applications: Frequency and Topology

Guillaume M. Matte, Paul L. M. J. Van Neer, Mike G. Danilouchkine, Jacob Huijssen, Martin D. Verweij, and Nico de Jong

Abstract—Second-harmonic imaging is currently one of the standards in commercial echographic systems for diagnosis, because of its high spatial resolution and low sensitivity to clutter and near-field artifacts. The use of nonlinear phenomena mirrors is a great set of solutions to improve echographic image resolution. To further enhance the resolution and image quality, the combination of the 3rd to 5th harmonics—dubbed the superharmonics—could be used. However, this requires a bandwidth exceeding that of conventional transducers. A promising solution features a phased-array design with interleaved low- and high-frequency elements for transmission and reception, respectively. Because the amplitude of the backscattered higher harmonics at the transducer surface is relatively low, it is highly desirable to increase the sensitivity in reception. Therefore, we investigated the optimization of the number of elements in the receiving aperture as well as their arrangement (topology). A variety of configurations was considered, including one transmit element for each receive element (1/2) up to one transmit for 7 receive elements (1/8). The topologies are assessed based on the ratio of the harmonic peak pressures in the main and grating lobes. Further, the higher harmonic level is maximized by optimization of the center frequency of the transmitted pulse. The achievable SNR for a specific application is a compromise between the frequency-dependent attenuation and nonlinearity at a required penetration depth. To calculate the SNR of the complete imaging chain, we use an approach analogous to the sonar equation used in underwater acoustics. The generated harmonic pressure fields caused by nonlinear wave propagation were modeled with the iterative nonlinear contrast source (INCS) method, the KZK, or the Burger's equation. The optimal topology for superharmonic imaging was an interleaved design with 1 transmit element per 6 receive elements. It improves the SNR by ~5 dB compared with the interleaved (1/2) design reported in literature. The optimal transmit frequency for superharmonic echocardiography was found to be 1.0 to 1.2 MHz. For superharmonic abdominal imaging this frequency was found to be 1.7 to 1.9 MHz. For 2nd-harmonic echocardiography, the optimal transmit frequency of 1.8 MHz reported in the literature was corroborated with our simulation results.

G. M. Matte, P. L. M. J. Van Neer, and M. G. Danilouchkine are with the Erasmus Medical Center, Biomedical Engineering, Rotterdam, The Netherlands.

J. Huijssen is with Katholieke Universiteit Leuven, Leuven, Belgium.

M. D. Verweij is with Technical University of Delft, Electromagnetic Research, Delft, The Netherlands.

N. de Jong is with the Cardiology Institute/University of Rotterdam, Biomedical engineering, Rotterdam, The Netherlands.

I. INTRODUCTION

SINCE its introduction in the late 90s, tissue 2nd-harmonic imaging of biological tissue has become the *de facto* standard in commercial echographic systems for medical diagnosis. The method is based on the selective imaging of the 2nd harmonic frequency [1], [2]. Compared with fundamental tissue imaging, tissue 2nd-harmonic imaging has a higher lateral resolution and lower side lobes, and is, therefore, less sensitive to clutter and off-axis scatters [3]–[6]. Also, because the 2nd-harmonic field builds up progressively, the effects of reverberation and near-field artifacts are greatly reduced [5]. Recently, Bouakaz *et al.* introduced a novel ultrasonic tissue imaging method dubbed superharmonic imaging (SHI) [7]. This technique combines the 3rd to 5th harmonics to construct an image. Tissue SHI efficiently suppresses near-field artifacts, reverberations, and off-axis artifacts in addition to the enhanced lateral and axial resolution. The resulting images showed more details than those produced by 2nd-harmonic imaging [7]. However, one of the challenges in SHI is the very wide bandwidth requirement (>130%) for the array used to transmit at the fundamental and receive the 3rd to 5th harmonic signals.

One approach for making such a very wideband transducer is to use capacitive micromachined ultrasound transducers (cMUTs). CMUTs having a −6-dB bandwidth of 130% have been reported [8], [9]. However, cMUTs are held back by challenges such as their inherent nonlinearity and relatively high crosstalk [8], [10]. The most important drawback of cMUT's for tissue SHI is their nonlinearity at high output pressures. The level of the higher harmonics generated by nonlinear propagation is low, thus any transmission of harmonics caused by device nonlinearity will considerably reduce the dynamic range of the imaging system.

The other way to obtain a transducer with sufficient bandwidth is to further improve the current transducer technology. However, the 130% bandwidth necessary for SHI is considerably larger than that achievable with conventional arrays. Although −6-dB bandwidths as high as 140% are reported in the literature for single-element transducers made from a 1–3 single crystal-epoxy composite, the actual peak bandwidth at −6-dB reported for single-crystal arrays are in the order of 95% [11]–[13]—not sufficient for SHI. Thus, to accommodate the bandwidth requirement for SHI, the transmit and receive elements

need to be separated. Such an approach has been proven to be viable and has been intensively treated in the scientific literature [14]–[20]. A short overview of the previously proposed solutions is given in the following paragraphs.

The first solution comprises a stacked topology. In this design, two active PZT layers with different resonance frequencies are placed on top of each other [14]–[16]. Thus, the total surface used for transmission and reception remains the same as in a conventional phased array. Advantages of this configuration are the limited total footprint of the array and the ease of manufacturing. The difficulty of using such a configuration comes from the electromechanical and acoustical coupling between the active layers. This causes troughs in the frequency response of the transducer caused by destructive interference in the active layers, if the resonance frequencies of both layers are close to each other. Although solutions have been presented in literature, they require either fairly complicated electronics or knowledge of the phase transfer function of each element [14], [15]. Moreover, the matching layer characteristic is compromised, because it should match for two different resonance frequencies.

A stacked topology for a single element has been described by Akiyama *et al.* [17]. Their design comprises an ultra-wideband transducer used in a mechanical sector scanner. It features a lead zirconate titanate (PZT) layer for transmission and a polyvinylidene fluoride (PVDF) layer for reception. To obtain very wide bandwidth, the PVDF layer functions below its resonance frequency. This has the added benefit of guaranteeing electromechanical decoupling between the active layers. However, the sensitivity of PVDF used in this manner is generally low.

Another option is to use a horizontal stack topology, in which two low-frequency arrays are positioned in the elevation direction on both sides of a central high-frequency array [18]. The main advantage of this approach is that the initial performance of the arrays is not modified, thus facilitating manufacture. Disadvantages are the limited overlap of the acoustic beams, constricting the imaging range, and the increased footprint in elevational direction.

A final possibility is to arrange the transmit and receive elements in the lateral direction. Bouakaz *et al.* [19] proposed interleaving two arrays, distributing the transmit and receive elements alternately. With this configuration, the transmit and receive beams fully overlap. Also, its footprint remains small and the transmit and receive elements can be optimized for their specific roles. Drawbacks are the relatively complicated manufacturing process and the intrinsically reduced sensitivity, because only half of the elements are used in reception and transmission. For transmission, the reduced sensitivity can be compensated by increasing the amplitude.

The interleaved design is chosen in our project. It has fully overlapping beams and a small footprint. Also, there is no direct electromechanical coupling between the elements, because the acoustic stacks for transmission and reception, including the associated circuitry, are fully separated. In addition to the initial reported interleaved array design [19], a follow-up interleaved array intended primarily for SHI and optimized for echocardiography was reported [20]. In that paper, the rationale behind the element geometry, frequency, and material choice was reported and performance measurements were provided. However, in the current paper, the interleaved design of alternating transmit and receive elements is further investigated. Redistributing the transmit and receive elements in groups or changing the ratio of transmit-to-receive elements may considerably improve the receive efficiency while retaining a high-quality beam. This is important for tissue SHI, because the level of the higher harmonics generated by nonlinear propagation is low. Moreover, the paper by van Neer *et al.* [20] only basically covers the choice for the 1 MHz transmit frequency used for the interleaved array optimized for superharmonic echocardiography. The optimal transmit frequency for tissue SHI depends on the level of the 3rd to 5th harmonics at the distances determined by the application. Consequently, the level of these harmonics is determined by two competing phenomena: nonlinear propagation and attenuation. To the authors' knowledge, no systematic study of the optimal transmit frequency for SHI versus the imaging distance required by the application has been conducted.

The first aim of this paper is to investigate the optimal transmit frequency for 2nd-harmonic imaging and SHI depending on the imaging application domain. The second aim of this paper is to optimize the distribution of the transmit and receive elements in groups or by changing the ratio of transmit-to-receive elements to maximize the receive sensitivity while retaining a high-quality ultrasound beam.

II. Research Directions

A. Transmit Frequency Optimization

The first part of the paper focuses on the optimization of the transmit frequency for multiple-harmonics imaging, initially for echocardiography but also extended to the different imaging ranges associated with other applications. To study the best possible compromise between the level of the 3rd to 5th harmonics received and the penetration depths associated with different applications, the transmit frequency has to be optimized. For this, we modify the sonar equation widely used in underwater acoustics for transducer design [21] to medical imaging purposes. This equation describes the whole pulse-echo imaging chain including transmit equipment, nonlinear wave propagation, backscattering, and receive equipment. The harmonic levels generated during the propagation of sound through tissue are calculated by two analogous methods described later.

B. Topology Optimization

The other part of the paper focuses on the optimization of the lateral distribution of the transmit and receive ele-
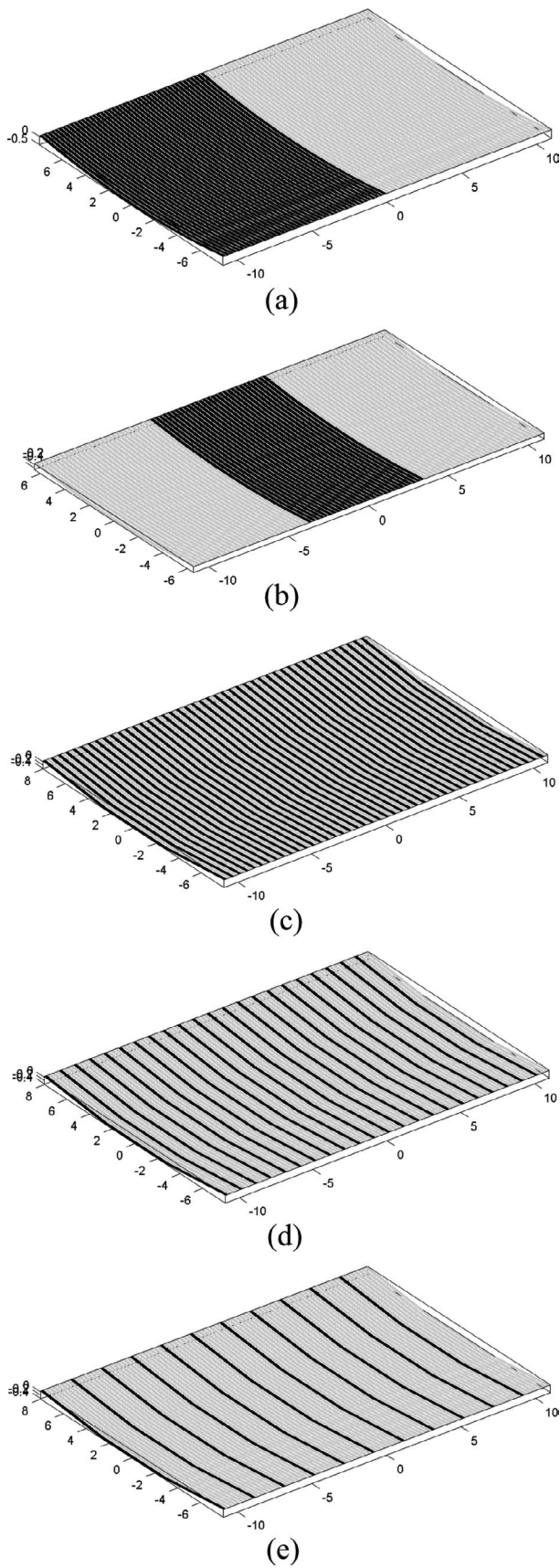
Fig. 1. Schematic view of various investigated topologies: (a) two-group topology, (b) three-group topology, (c) interleaved 1/2 topology, (d) interleaved 1/4 topology, (e) interleaved 1/8 topology. The black elements are used in transmission; the lightly colored elements are used in reception.

ments to improve the receive efficiency while retaining a high-quality ultrasound beam.

First we analyze an array where the ratio of transmit and receive elements is 1. The array with N elements is then divided in 2, 3, or N groups, so each group has $N/2$, $N/3$, or 1 element. The former cases are referred to as group topologies, and the last case is referred to as the interleaved or mixed topology. After this, the effects of lowering the ratio of transmit-to-receive elements is studied to increase the receive sensitivity. The decrease in sensitivity in transmission can be compensated by higher electrical transmission amplitudes. For the analyses, we used simulations based on Field II [22], [23] in combination with the Burgers equation [24] and the INCS method [25], [26].

C. Group Topology

In the first configuration of the group topology class, the array is constituted of two equal groups of elements distributed laterally [see Fig. 1(a)]. The transmit elements (tuned on the fundamental frequency) are on one side of the array, whereas the receive elements (tuned on higher-frequency components) are on the other side. The origin of the coordinate system of the probe is located between both groups of elements.

The second type of the group topology defines an array consisting of three parts in a lateral distribution [see Fig. 1(b)]. A group of transmit elements is located in the middle and two groups of receive elements are laterally arranged on each side of the transmit elements. The total number of receive elements is twice the number of transmit elements. This configuration is analogous to the one described by Ferin [18], except in our case the lateral arrangement of the elements enables electronic focusing instead of a fixed focus. The transmit and receive elements are distributed symmetrically, thus the convolved transmit and receive beams are expected to be symmetric.

D. Interleaved Topology

The interleaved topology is an array configuration where single transmit elements are equidistantly placed over the footprint [see Figs. 1(c)–1(e)]. The successive transmit elements are interleaved by a group of n receive elements ($n = 1$ to N). We further refer to $1/k$ interleaved topology to make distinction between each particular combination of a single transmit element and $n = k - 1$ receive elements. The main difference between the introduced topology classes lies in the fact that transmit elements are grouped together to form the transmit aperture in the group topology class. The perceived advantage of the interleaved over the group topology is the possibility of increased sensitivity in reception while having the best distribution of the elements from a beam-quality perspective. According to the nomenclature established in the current paper, the transducer design described by Bouakaz *et al.* [19] and van Neer *et al.* [20] belongs to the 1/2 interleaved topology.

E. Criteria for Topology Evaluation

Of major importance in the design of phased arrays for medical ultrasound is the system dynamic range. It is limited by the relative energy difference between the main and the grating lobes and by the SNR. A grating lobe is the result of constructive interference of the acoustic waves produced by the array in a lateral direction. The backscattered echoes originating from a grating lobe pollute the signal of the main beam. The grating lobes are caused by the under-sampling of the physical aperture. Considering a phased array as a sampled aperture and taking into account the Nyquist theorem, it is easy to deduce that a grating lobe would occur when the distance between neighboring elements of the array exceeds half the wavelength of the emitted pulse. Thus, the presence of a grating lobe and its intensity depend on the wavelength and the pitch. Obviously to avoid the occurrence of grating lobes, the inter-element spacing should be equal to or less than half the wavelength of the pulse. In the case of harmonic imaging, this requirement can be relaxed because the production of the nth harmonic is related to the pressure in the beam to the power n; the peak pressure in the main beam will be considerably higher than the pressure in the grating lobe. The pressure in the grating lobe relative to the pressure in the main beam at the frequency used to construct an image sets a limit on the dynamic range of that image. Cobbold [24] states that the grating lobe pressure should be 40 dB below the pressure in the main beam.

To evaluate the effect of the varying distance between elements for each topology, the levels of a harmonic in the main and grating lobe have to be calculated and compared with each other. All further analyses will be backed by simulations based on Field II [22], [23] in combination with the Burgers equation [24], the KZK equation [27], and the INCS method [25], [26].

III. Theory

A. Expression of the SNR

The SNR can be expressed as a logarithmic sum of transfer functions affecting the signal, each representing a phenomenon of the imaging process:

$$\mathrm{SNR}(\omega) = V + \mathrm{Te}(\omega) + H_{\mathrm{FORWARD}}(\omega) - \mathrm{Bs}(\omega) \\ - H_{\mathrm{BACKWARD}}(\omega) + \mathrm{Hs}(\omega) - \mathrm{Ns}, \quad (1)$$

where V is the excitation amplitude on the transducer clamps, expressed in decibels relative to 1 V; Te is the transmit efficiency expressed in decibels relative to 1 Pa/V, which is analogous to the transmitting voltage response (TVR) in underwater acoustics; H_{FORWARD} is the function describing the change of the pressure wave during forward propagation, expressed in decibels, and includes diffraction, the focal gain, attenuation, and nonlinearity;
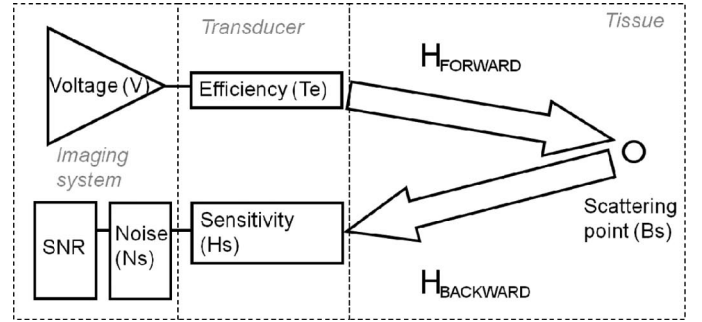

Fig. 2. Schematic description of Eq. (1) for calculating the SNR.

Bs corresponds to the loss of power during the backscattering process and is analogous to the target strength in underwater acoustics, expressed in decibels; H_{BACKWARD} is the function describing the pressure wave during back propagation. By assuming linear back propagation, it includes only frequency dependent attenuation (A) and is expressed in decibels; Hs is the receive sensitivity of the transducer expressed in decibels relative to 1 V/Pa; and Ns is the noise of the imaging system expressed in decibelsrelative to 1 V. This expression is analogous to the sonar equation, widely used in underwater acoustics for transducer design [21].

The combination of V, Te, and H_{FORWARD} is the incoming pressure at the scatterer location. Thus, (1) can be rewritten into:

$$\mathrm{SNR}(\omega) = P(\omega) - \mathrm{Bs}(\omega) - A(\omega) + \mathrm{Hs}(\omega) - \mathrm{Ns}, \quad (2)$$

where P is the incoming pressure at the scatterer location by forward propagation of the ultrasound produced by the transducer, expressed in decibels relative to a plane wave of 1 Pa; A is ultrasound attenuation during linear back propagation to the transducer, expressed in decibels; and ω is the angular frequency.

Fig. 2 provides a schematic for the concept of the expression of the SNR. The terms in (2) are explained in more detail in the following paragraphs.

B. The Incoming Pressure at the Scatterer Location (P)

For nonlinear propagation, the acoustic wave at the transducer surface has to be propagated toward the scatterer location. We use two simulation models: the KZK equation [27]–[29] and the INCS approach [25], [26]. These models include the attenuation of the medium. P is expressed in decibels relative to 1 Pa.

C. The Excitation Voltage (V)

The excitation voltage (V) over the clamps of the transmit part of the transducer is expressed in decibels relative to 1 V.

D. The Transmit Efficiency (Te)

The transmit efficiency (Te) is defined as [30]

$$\text{Te} = \frac{|p_0|}{|V_\text{T}|}, \qquad (3)$$

where p_0 is the pressure at the transducer surface and V_T is the voltage over the transducer electrodes. Te is expressed in decibels relative to 1 Pa/V.

E. The Backscattered Signal (Bs)

The total backscattered intensity (Bs) is defined as

$$\text{Bs} = \Omega \mu_t L, \qquad (4)$$

where Ω is the solid angle, impinging the receive aperture of the transducer for a given observation point. The area of the receive aperture is simply determined as a product of an element area and the number of elements in reception. L defines the scattering distance, which is equal to the distance between the observation point and the transducer, and μ_t is the scattering cross-section, which is modeled as [31]:

$$\mu_t = \mu_a \cdot f^{\mu_b}, \qquad (5)$$

where f is the frequency, μ_a in cm^{-1}·Sr^{-1} (described in Duck as a), and μ_b is associated with the frequency dependency (described in Duck as b).

Bs is expressed in decibels.

F. Attenuation of Backscattered Signal During Backpropagation (A)

The amplitude of the backscattered signal is generally low; thus, the backward propagation can be considered to be linear. The attenuation of the backscattered signal during linear propagation of the backscattered signal from the tissue target to the transducer (A) was modeled as

$$A = r \cdot \alpha_0 \cdot f^b, \qquad (6)$$

where α_0 is the frequency attenuation factor, r is the distance from the transducer, and b is associated with the frequency dependency. A is defined per harmonic n in decibels.

G. The Receive Sensitivity (Hs)

The receive sensitivity (Hs) is defined as [30]

$$\text{Hs} = \frac{|V_\text{T-open}|}{|p_a|}, \qquad (7)$$

where $V_\text{T-open}$ is the open circuit voltage over the transducer and p_a is the pressure received on the transducer surface. Hs is expressed in decibels relative to 1 V/Pa.

H. Transducer and System Noise (Ns)

The transducer and system noise was expressed in decibels relative to 1 V. The noise is assumed to be white.

Because the SNR is considered after beam forming, the noise level is divided by $\sqrt{N_{el}}$.

I. The KZK Equation

The cumulative effects of diffraction, absorption, and nonlinearity in directive sound beams are modeled by the KZK nonlinear wave equation [1], [24]. The KZK equation uses the parabolic approximation and is therefore only valid for 15° around the direction of the wave propagation.

$$\frac{\partial^2 p}{\partial z \partial t'} = \frac{c_0}{2}\left(\frac{\partial^2 p}{\partial r^2} + \frac{1}{r}\frac{\partial p}{\partial r}\right) + \frac{\alpha_0}{\omega_0{}^2}\frac{\partial^3 p}{\partial t'^3} + \frac{\beta}{2\rho_0 c_0{}^3}\frac{\partial^2 p}{\partial t'^2}, \quad (8)$$

where p is the sound pressure; t' is the retarded time, defined as $t' = t - z/c_0$; c_0 is the small-signal acoustic velocity; r is the transverse radial coordinate; α_0 is the thermoviscous attenuation coefficient, ω_0 is the angular frequency of the fundamental, β is the coefficient of nonlinearity; and ρ_0 is the ambient density.

The first term on the right-hand side of (8) accounts for diffraction, the second term accounts for absorption and the third term accounts for quadratic nonlinearity. To mimic tissue absorption, the absorption term was replaced with an attenuation term which depended linearly on the frequency [7]. Eq. (8) is written using cylindrical coordinates, which implies axi-symmetry—also in the source—and it uses a paraxial approximation. The well-known time domain approach proposed by Lee and Hamilton was implemented [27]–[29].

The KZK equation has been used by many researchers and is in excellent agreement with experiments [32], [33].

J. The INCS Method

A full-wave description of the nonlinear propagation of acoustic waves in a homogeneous medium is given by the Westervelt equation [28]. The INCS method provides a numerical solution for this equation and is not dependent on the direction of the wave propagation:

$$\frac{1}{c_0{}^2}\frac{\partial^2}{\partial t^2}[\chi(t) *_\text{t} p] - \nabla^2 p = S + \frac{\beta}{\rho_0 c_0{}^4}\frac{\partial^2 p^2}{\partial t^2}, \qquad (9)$$

where $\chi(t)$ is a normalized compressibility relaxation function, $*_\text{t}$ is the convolution with respect to time, and S is the primary source term. The usual prescription of a pressure $P(x, y, t)$ at the boundary $z = 0$ can be accounted for by using $S = -\partial[F(x, y, t)\delta(z)]/\partial z$, where $F = 2P(x, y, t)$ is the surface force density in the positive z-direction and $\delta(z)$ is the Dirac delta function. The strategy to solve this equation is to consider the nonlinear pressure field as a sum of the linear field solution and a nonlinear correction. The linear field solution can be obtained from the homogeneous lossy and linear background medium with external source S. The nonlinear field correction arises from the

TABLE I. Aperture Characteristics and Acoustic Medium Properties Used for the Simulations.

Simulation	Element length [mm]	Element width [μm]	Number of elements	c_0 [m/s]	ρ [kg/m³]	Kerf [μm]	Steering angle [°]	Pulse length	Absorption [Np·m⁻¹·MHz⁻ᵇ]		Scattering [cm⁻¹·Sr⁻¹]		β
									α_0	b	μ_a	μ_b	
Frequency SNR simulation	16	200	44	1580	1050	50	0	3 cycles	5.2	1.01	$2.7 \cdot 10^{-4}$	1.2	4.4
Topology: Complete fundamental pressure field	16	200	—	1490	1000	50	35	3 cycles	25.10^{-3}	2	—	—	3.5
Topology: Calculation of the harmonic grating lobe level	16	200	—	1580	1050	50	/	3 cycles	5.2	1.01	—	—	4.4

solution of (9) with the single second term on the right-hand side. Those solutions are numerically refined in an iterative manner until convergence. The non-quadratic attenuation of lossy media like tissue was incorporated. More details on the INCS method can be found in the works of Huijssen *et al.* [25], [26], [34].

In contrast to the KZK simulations, the INCS method does not require a paraxial approximation. As such it is more precise for steered beams, but requires considerably more computation time and memory resources.

K. Linear Acoustic Modeling Using Field II

The FIELD II simulation program [22], [23] was used to calculate the fundamental acoustic fields of the various group configurations and mixed configurations. The Burgers equation was used to estimate the harmonic level in the grating lobes.

L. The Burgers Equation

The Burgers equation describes the propagation of finite-amplitude plane progressive waves in a medium with thermoviscous losses. The solution was found as a complex Fourier series using the iterative computation scheme given by Cobbold [24].

IV. Material and Methods

A. Transmit Frequency Optimization

Nonlinear propagation is frequency dependent. In general, at higher frequencies wave propagation is more nonlinear and therefore more harmonics are generated. On the other hand, the attenuation also increases at higher frequencies, which counterbalances the generated harmonics. The SNR of the harmonics depends on the transducer configuration and the characteristics of the propagating medium.

See Table I for values used in the simulations. The SNR as a function of the frequency is given by (2). We used liver

as the propagation medium ($c_0 = 1580$ m/s, $\rho = 1050$ kg/m³ and $\beta = 4.4$, $\mu_a = 2.7 \times 10^{-4}$ m⁻¹·Sr⁻¹ and $\mu_b = 1.2$, $\alpha_0 = 5.2$ Np·m⁻¹·MHz⁻ᵇ and $b = 1.05$ [31]). The transducer was the interleaved array reported by van Neer *et al.* [20]. This phased array transducer had a low-frequency subarray consisting of 44 elements (16×0.2 mm, center frequency of 1 MHz) interleaved with a high-frequency subarray also consisting of 44 elements (13×0.2 mm, center frequency of 3.7 MHz). The pitch was 0.5 mm, and so the lateral dimension of the array was 22 mm. The elevation focus was fixed and set to 60 mm. In the lateral direction, the steering angle was set to zero and the focal distance to 60 mm. The transmit efficiency (Te) was taken as 32.5 kPa/V and the receive sensitivity (Hs) was taken as 21 μV/Pa [20]. The transducer and system noise was measured and equal to 7 μV_RMS. The measurement was performed using the previously mentioned interleaved array transducer mounted on a tissue-mimicking phantom combined with a commercial ultrasound system. A series of time traces was recorded with the receive amplifiers on their maximum settings, while the transmitters were turned off. The time traces were filtered over a 3.5-MHz band and from this, the RMS voltage was calculated. The excitation amplitude on the transducer was chosen to get a resulting MI in focus of 1.5 (note: the MI is equal to the peak negative pressure divided by the square root of the frequency). The MI was used as an equalization reference, as it is widely used, and reported on-screen in all ultrasound scanners (although this does not describe nonlinear processes during wave propagation).

The value of every individual harmonic in P was computed using either the KZK equation or the INCS method. The KZK equation for an axisymmetric lightly focused source was solved in the time domain according to the algorithm described by Lee and Hamilton [27]. The algorithm was implemented in C and an interface was written in Matlab to extract the data [35].

The solver of the INCS method has been implemented in parallel and ran on an IBM clustered symmetric multiprocessing system (Huygens system, Amsterdam, The Netherlands). The entire system consists of 1664 dual core processors (IBM Power6, 4.7 GHz, IBM, Armonk, NY),

128 Gbytes/256 Gbytes of memory per node. The total peak performance is 60 Tflop/s. Depending on the frequency, a single run takes 2 to 30 h on 32 processors for a complete 3-D nonlinear beam profile.

B. Topology Optimization

For the topology, the discriminating feature is the grating lobe level. Simulations have been carried out to calculate the fundamental and harmonic main beam together with the side lobes and grating lobes. For the simulations, we used a Gaussian apodized transmission signal of 3 cycles with a frequency of 1.2 MHz. This frequency corresponds to the optimal transmit frequency for SHI and echocardiography (see the results of the frequency optimization part). For the propagation medium, we used the properties of liver: $c_0 = 1580$ m/s, $\rho = 1050$ kg/m^3. The linear simulations were lossless; for the nonlinear simulations $\beta = 4.4$, $\alpha_0 = 5.2$ Np·m^{-1}·MHz^{-b}, and $b = 1.05$ [31] were used. The excitation amplitude was set to get an MI of 1.5 in focus. Fig. 1 shows schematic examples of the apertures used. The beam steering angle was 35° and the lateral and elevation foci were set to 60 mm.

A two-step approach was used to calculate the grating lobe levels. First, the fundamental acoustic field was calculated using the FIELD II simulation program [22], [23]. Second, the harmonic grating lobes were estimated from the fundamental grating lobe levels using the Burgers equation. For that, the fundamental peak pressure in the grating lobe was used as the starting pressure for the Burgers equation. The wave was then propagated over a distance of 60 mm. Acoustic attenuation was included. The harmonic levels of the grating lobes were compared with the harmonic levels in the main beam as calculated using INCS simulations for the same apertures.

V. Results

A. Transmit Frequency Optimization

In Fig. 3(a), the SNR of the system as function of the transmit frequency is plotted for the fundamental through the 5th harmonic. The curves are calculated at a depth of 6 cm. As seen in the figure, the SNR of the fundamental ranges between 62 and 79 dB for the transmit frequency range of 0.5 to 2.5 MHz. The 2nd-harmonic SNR ranges between 47 and 70 dB, the 3rd-harmonic SNR between 30 and 61 dB, the 4th-harmonic SNR between 13 and 53 dB, and the 5th-harmonic SNR between −2 and 45 dB. For H1, there is no maximum observed between 0.5 and 2.5 MHz; the optimal transmit frequency is higher than 2.5 MHz. There is a maximum observed for the 2nd, 3rd, 4th, and 5th harmonics. For the 2nd harmonic (H2), the maximum occurs at 2.1 MHz; for the 3rd harmonic (H3), around 1.9 MHz; for the 4th harmonic (H4), around 1.85 MHz; and for the 5th harmonic (H5), around 1.75 MHz. In Fig. 3(a) the results of the KZK and the INCS simulations are
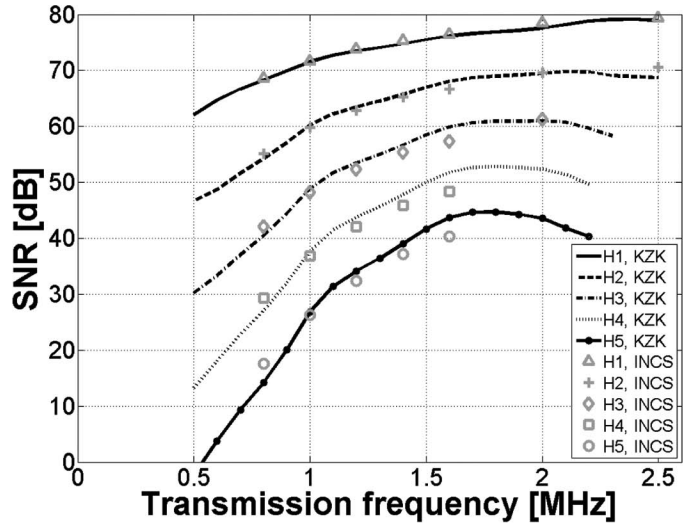
(a)
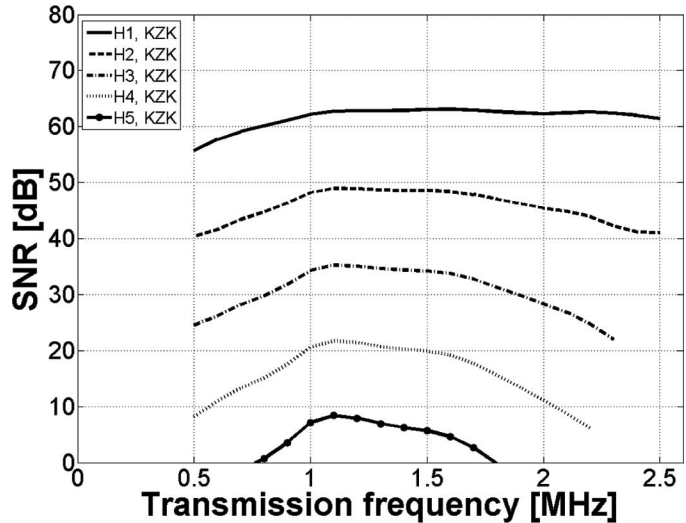
(b)

Fig. 3. (a) The SNR of the fundamental (H1), 2nd (H2), 3rd (H3), 4th (H4), and 5th (H5) harmonics depending on the transmission frequency as calculated at an axial distance of 6 cm using the INCS method and the KZK model based on the same input parameters. The properties of the homogeneous medium were based on those of liver. (b) The SNR of the fundamental (H1), 2nd (H2), 3rd (H3), 4th (H4), and 5th (H5) harmonics depending on the transmission frequency as calculated at an axial distance of 10 cm using the KZK model. The properties of the homogeneous medium were based on those of liver.

plotted. In the frequency range from 0.8 through 1.4 MHz, the two methods differ only by ± 1 dB for the fundamental up to the 3rd harmonic, whereas this is slightly higher for the 4th and 5th harmonic (±2 dB). The maximum difference between the INCS method and the KZK method is ± 3 dB. These slight differences are as expected for an unsteered beam. The KZK method is used for most of the remainder of this article.

Fig. 3(b) shows the SNR for each harmonic as calculated using the KZK method at an imaging depth of 10 cm. Two effects can be seen when comparing these results with those obtained at the 6 cm imaging depth shown in Fig.
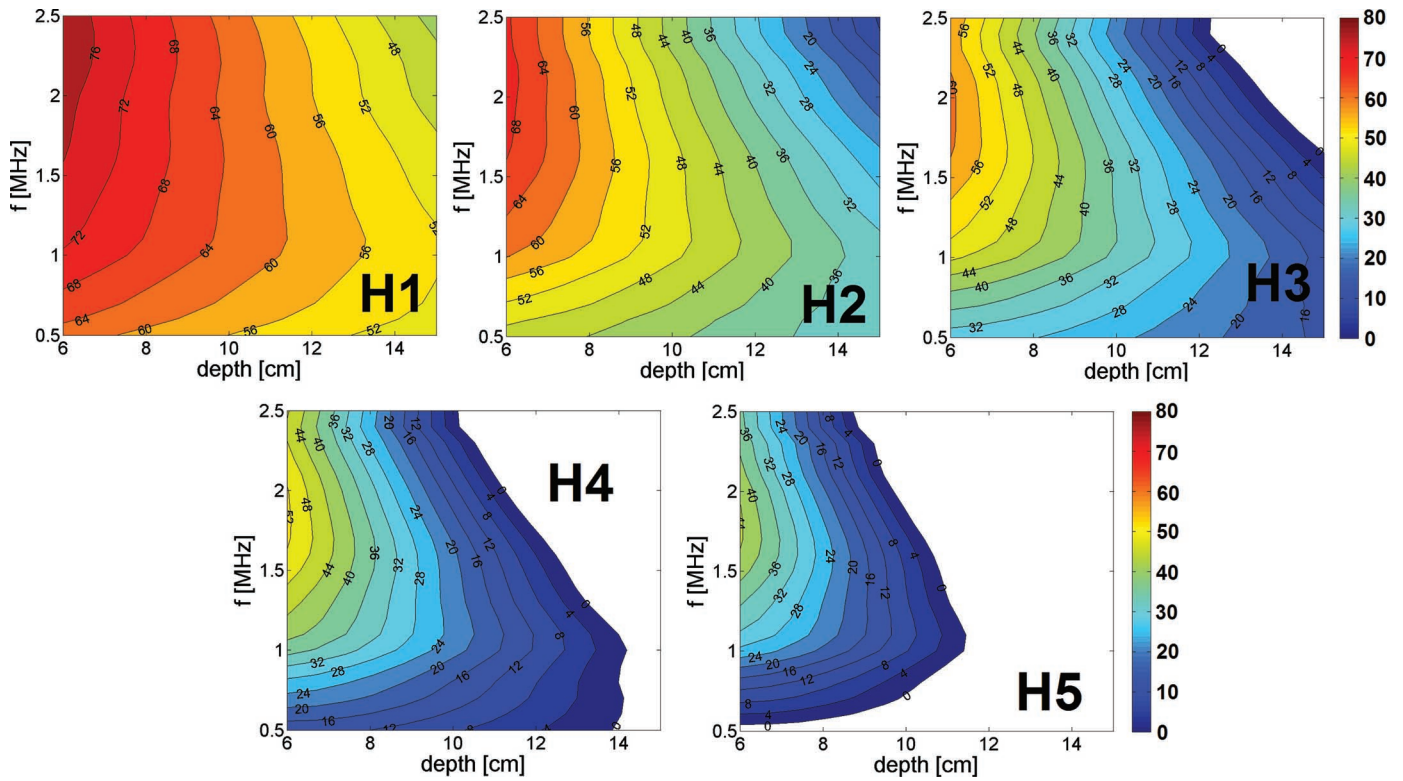
Fig. 4. The SNR depending on the transmission frequency and depth. Panel H1 shows the fundamental frequency, panel H2 details the 2nd harmonic, panel H3 displays the 3rd harmonic, panel H4 shows the 4th harmonic, and panel H5 details the 5th harmonic. The SNR level is indicated by a color scale with an 80-dB dynamic range.

3(a). First, the level of the curve is lower over the whole frequency band, and second, the maximum of the curves shifts toward lower frequencies. Because the foci of all the harmonics are at or around 6 cm, both phenomena can be explained by the increased propagation path and consequently the increased attenuation. The fundamental has an SNR of 62 dB and is flat for frequencies above 1 MHz, so for fundamental imaging the preferred frequency is 2.5 MHz or higher. The harmonics show all a maximum around 1.2 MHz. H2 and H3 have an SNR above 30 dB, whereas the SNR of H4 is above 20 dB. For the 5th harmonic, the level is further decreased and is less than 10 dB above the noise level.

In diagnostic ultrasound, the transmit frequency used depends on the application and therefore on the scanning depth. If the scanning depth increases, the transmit frequency is lower. In Fig. 4, intensity plots show the SNR levels in decibels as a function of the transmit frequency and scanning depth assuming a flat (frequency independent) response of the transducer. From the figure, it can be seen that at a scanning depth of 6 cm, the most optimal transmit frequency in terms of SNR for fundamental imaging is higher than 2.5 MHz. However, at a scanning depth of 12 cm, the highest SNR for the fundamental is at a transmit frequency of 1 MHz. For the 3rd harmonic and a scanning depth of, for example, 12 cm, a transmit frequency of 1 MHz results in an SNR of more than 25 dB (light blue in the online figure), but is close to 0 dB for a transmit frequency of 2 MHz (dark blue in the online fig-

ure). The 4th and 5th harmonics only have an acceptable SNR at scanning depths smaller than 8 cm.

B. Topology Optimization

Several of the investigated topologies of the array transducer are plotted in Fig. 1. The transmit elements are black; the receive elements have a light color. The transmit elements always transmit at the fundamental frequency (1.2 MHz). In the left column of Fig. 5, the transmit-receive beam profiles for the fundamental frequency are shown. In this case, the transmit elements are also receiving the fundamental. The right column in Fig. 5 shows the convolution of the transmit ultrasound field at the fundamental frequency and the receive ultrasound field at the 2nd harmonic frequency. The steering angle is 35°. Of importance are the main beam size and the off-beam energy, mostly reflected in the side lobes and grating lobes.

C. Two-Subarray Topology

The two-subarray topology is shown in Fig. 1(a). The transmit elements are on one side of the array (black); the receive elements are on the other side (light color). The left panel of Fig. 5(a) shows the convolved transmit-receive beam at the fundamental frequency. The fundamental beam width at focus is 8.7 mm and the 2nd-harmonic beam width is 4.4 mm [see the right panel of Fig. 5(b)].
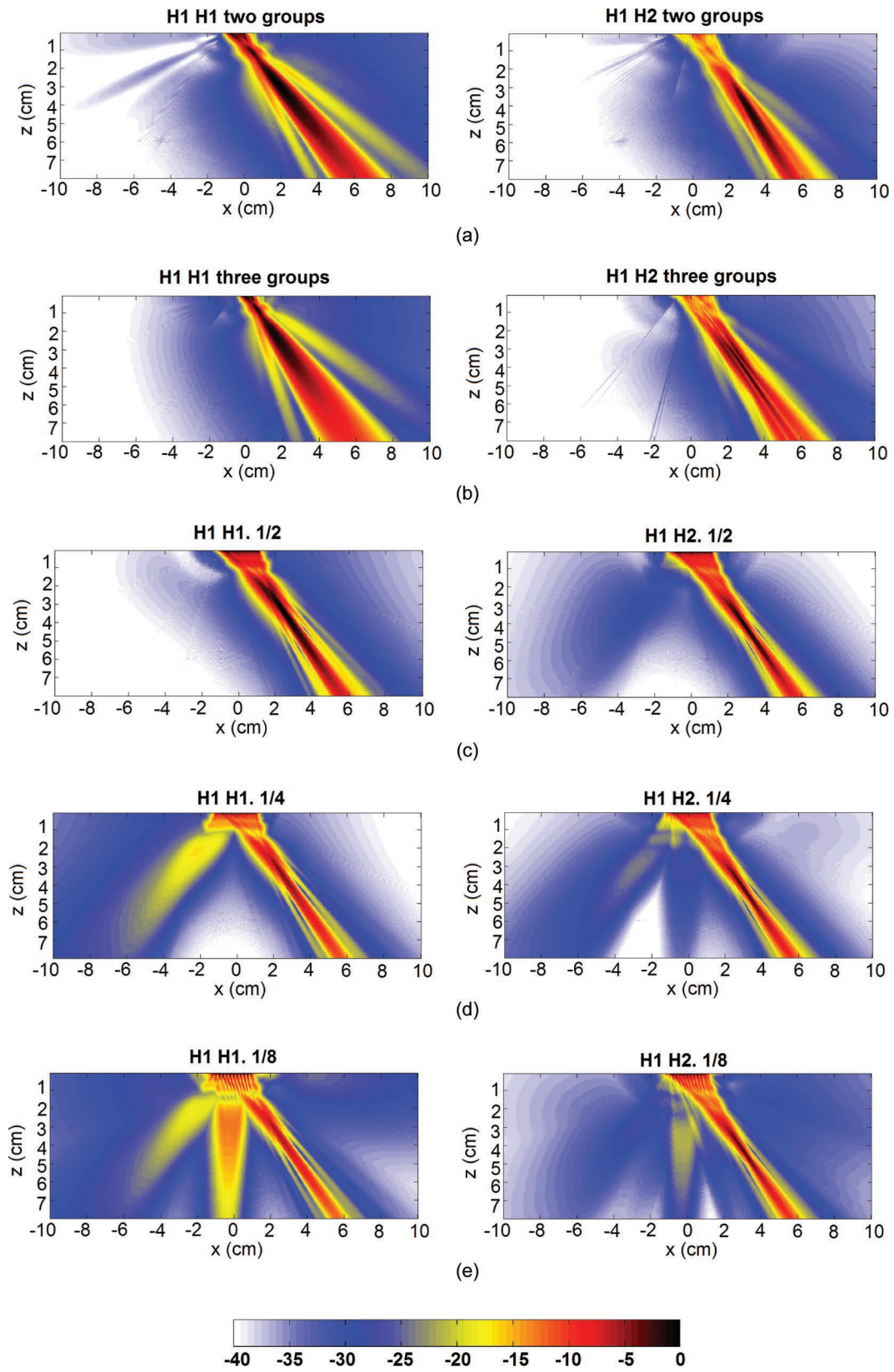
Fig. 5. Convolved transmit-receive beams produced by the considered topologies. Left plots: transmit fundamental, receive fundamental (only the black apertures shown in Fig. 1). Right plots: transmit fundamental, receive 2nd harmonic. The intensity in decibels is denoted using a color scale with a 40-dB dynamic range. (a) Two-group topology, (b) three-group topology, (c) interleaved 1/2 topology, (d) interleaved 1/4 topology, (e) interleaved 1/8 topology.

TABLE II. Peak Grating Lobe Intensity Relative to Peak Main Beam Intensity of the Mixed/Interleaved Topologies.

f_0 [MHz]	Pitch	Number of receivers	Fundamental	2nd Harmonic	3rd Harmonic	4th Harmonic	5th Harmonic
1.2	1/2	44	—	—	—	—	—
	1/3	59	−23	−56	−83	−107	−130
	1/4	66	−15	−41	−59	−76	−92
	1/5	70	−13	−36	−50	−64	−77
	1/6	73	−11	−32	−46	−57	−69
	1/7	75	−9	−30	−42	−53	−62
	1/8	77	−8	−27	−37	−47	−55

Note that the convolved transmit (fundamental)-receive (2nd harmonic) beam is curved. This effect becomes more pronounced for the higher harmonics because the receive beam itself becomes narrower for higher frequencies.

D. Three-Subarray Topology

The three-subarray topology is detailed in Fig. 1(b). The transmit part is in the center and the two receive parts are located on each side of the transmit array. The fundamental transmit-receive beam is displayed in the left panel of Fig. 5(b); the convolved fundamental transmit and 2nd-harmonic receive beam is displayed in the right panel of Fig. 5(b). The fundamental beam is much wider (11.2 mm) than the previous configuration as a result of the smaller aperture. The 2nd-harmonic beam on the right measures 7.3 mm at focus. Around the focal point, the 2nd-harmonic beam contains multiple peaks in the lateral cross-section, which is orthogonal to the main direction of the wave propagation. This shape is analogous to a beam having a very high level of side lobes (up to −2 dB relative to its center).

E. Mixed Topology

The mixed or interleaved topologies of the array are further shown in Figs. 1(c)–1(e). The interleaving ratio varies from one transmit element for each receiving element [denoted 1/2, see Fig. 1(c)], up to a ratio of one transmit element for every seven receive elements [denoted 1/8, see Fig. 1(e)]. The fundamental transmit-receive beams are displayed in the left panels of Figs. 5(c)–(e); the convolved fundamental transmit and 2nd harmonic receive beam are displayed in the right panels of Figs. 5(c)–(e). For the 1/2 configuration there are no grating lobes visible for the fundamental beam and consequently also the 2nd harmonic beam is free of grating lobes [see Fig. 5(c)]. This changes for the 1/4 configuration shown in Fig. 5(d). There is a clear grating lobe in the fundamental beam plot located at about −35°. In the 2nd-harmonic beam profile, the grating lobe level is greatly diminished and just above the noise level. For the 1/8 configuration in Fig. 5(e), there are two grating lobes, one at −35° and the other one at 0°. The one at 0° is only −10 dB below the main beam intensity. For the 2nd-harmonic beam the grating lobe is still there, but its peak level is now at −20 dB. The main beam in

the mixed topologies is more or less independent of the interleaving ratio, because the aperture remains the same. The fundamental beam width at 6 cm is 7.8 mm.

The ratios of the peak grating lobe and peak main beam intensities of the mixed topologies are shown in Table II for the fundamental through the 5th harmonic. According to Cobbold [24], an imaging system should have a grating lobe to main lobe level of less than −40 dB. From Table II, it can be observed that the maximum interleaving ratio of the transmit-receive elements is 1/2 for fundamental imaging. For the 2nd harmonic, the maximum ratio is 1/4, and for the 3rd harmonic, a ratio of 1/7 still provides a peak grating lobe to peak main lobe ratio below −40 dB. For the 4th and 5th harmonics, the grating lobe to main beam levels remain below −40 dB in all configurations.

VI. Discussion

A. Transmit Frequency Optimization

The results presented in this paper allow for the validation of the findings on the optimal transmit frequency for 2nd-harmonic imaging but also for the prediction of the same parameter for imaging based on higher harmonics. Kasprzak *et al.* [36] investigated experimentally the optimal transmit frequency for 2nd-harmonic imaging. Their methodology consisted of comparing the quality of the images produced by several commercial echographic systems on the frequency range of 1.6 to 1.8 MHz and 2.1 to 2.4 MHz. A relatively low transmit frequency of 1.6 to 1.8 MHz was found to be necessary to visualize the whole heart, including the parts furthest away from the transducer. We translate the qualitative criteria used by Kasprzak *et al.* into an explicit demand for the dynamic range at the maximum imaging depth depending on the transmit frequency. For a given distance, the aim is that the signal with the highest possible frequency still satisfies the dynamic range criterion. In the case of echocardiography, we analyze our results at 12 to 15 cm, requiring at least 30 dB dynamic range at this distance. Indeed our simulation results confirm the initial findings of Kasprzak *et al.* [36] and show that the optimal transmit frequency is ~1.7 MHz for 2nd-harmonic echocardiography (see Fig. 4); this provides an SNR at 13 cm of 32 dB. The optimal transmit frequency for the selective imaging of the

3rd harmonic is 1.0 to 1.2 MHz (see Fig. 4). However, with a 3rd-harmonic SNR of ~22 dB at 13 cm, it is below the 30 dB dynamic range criterion. Neither the 4th nor the 5th harmonics would provide sufficient dynamic range at 13 to 15 cm for the selective imaging using either. Because the 3rd harmonic contains the most energy of the components in the superharmonic band, the optimal transmit frequency for superharmonic echocardiography is concluded to be 1.0 to 1.2 MHz (see Fig. 4). Although the 4th and 5th harmonics are below the noise floor at 14 to 15 cm, they still contribute to the superharmonic image at shallower depths. The optimal transmit frequency found for SHI is in agreement with the 1.0 MHz reported previously [20].

The maximum imaging depth for imaging of the kidneys, the gallbladder, or the abdominal aorta is at 9 to 10 cm, which is lower than that for echocardiography. Therefore, the optimal transmit frequency for 2nd-harmonic imaging is at ~2.5 MHz also higher (see Fig. 4). For 3rd-harmonic imaging, the optimal transmit frequency becomes ~1.7 to 1.9 MHz. For imaging based on the 4th harmonic, the optimal transmit frequency is ~1.6 MHz, but the harmonic level remains below the required 30 dB dynamic range threshold with a minimum SNR of 22 dB at 10 cm (see Fig. 4). The optimal transmit frequency for SHI is ~1.8 MHz, because the 3rd harmonic component contains the most energy of the components in the superharmonic band. Both the 4th and 5th harmonics are above the noise floor and contribute to the superharmonic image.

The simulations detailed here were performed for a homogeneous medium using the material properties reported for liver. However, the human body has a heterogeneous structure with considerable variation in tissue material properties and interfaces in between different tissue types, where the acoustic impedances vary strongly. For example in the case of echocardiography, most of the propagation medium consists of blood and cardiac tissue. Although the range of reported B/A and attenuation values for cardiac tissue are similar to those reported for liver, the attenuation values reported for blood are four times lower than that of liver tissue at similar B/A values [31]. Therefore, the SNR levels reported here should be interpreted as a worst-case scenario.

Also, the element geometry used for the simulations was based on the geometry reported for a transducer intended for echocardiography. In this modality, the height and width of the transducer is limited by the space between the ribs. However, in abdominal imaging there is no such constraint and the element dimensions and number of elements can be increased. This would increase SNR but the reported trends would remain similar.

B. Topology Optimization

The convolved transmit(fundamental)-receive(harmonic) beam is curved in the case of the two-groups topology. This is caused by the fact that the centers of the transmit and receive apertures do not spatially coincide. The contribution of the farthest elements to the focal point is overestimated, which places the effective backscattered signal at an incorrect position in space. The solution requires modified element delays for steering in transmission and an extra post-processing step to correct for the abberated point spread functions in reception. The three group topology does not have the aforementioned problems, but the convolved transmit-receive beam is wide. At the limit of the large group topology is the interleaved topology. Its convolved transmit-receive beam is the most narrow and well defined. Therefore, the fully interleaved design is preferred over topologies consisting of a lower number of groups.

The mixed topologies combine the well-defined beams of the interleaved design with an increase in surface area dedicated for receiving. The dynamic range of an ultrasound system is limited by the grating lobe to main lobe ratio and the maximum SNR, where the lower of the two is the main determinant. Cobbold [24] states that the grating lobe pressure should be 40 dB below the pressure in the main beam. Focusing on the 3rd harmonic, our simulations show that the 1/7 configuration provides the maximum number of receive elements while still providing a grating lobe level less than −40 dB compared with the main beam (see Table II). For the 4th and 5th harmonics, all configurations provide sufficiently low grating lobe levels. Because the 3rd harmonic has the highest intensity overall of the superharmonics (3rd to 5th harmonics), the 1/7 configuration is optimal for superharmonic echocardiography.

The optimal 1/7 configuration uses 75 elements for reception, compared with the 44 elements used in reception by the interleaved (1/2) configurations reported in previous papers [19], [37]. The increased number of receive elements improves the total SNR by ~5 dB, because of the reception of an increased amount of backscattered energy and the reduction of the effective noise level after beamforming. The effect can be observed in the SNR values reported for the 5th harmonic in Table III: the SNR at 6 cm increases from 32 dB for the 1/2 configuration to 37 dB for the 1/7 configuration. Although a 5 dB improvement in SNR may seem like a modest improvement, it is an SNR improvement over the entire imaging depth.

The main assumption here is that the voltage over the transducer clamps, or the transmit efficiency of the transmit elements, can be increased sufficiently to compensate for the reduced number of transmit elements. Van Neer *et al.* reported reaching an MI of 1.9 by exciting their 1/2 transducer using signals of 60 V in amplitude [20]. Thus, to reach the same peak pressures using the 1/7 configuration, the amplifier output should be increased to an amplitude of 210 V. This voltage level should pose no problem to the integrity of the piezomaterial at the thicknesses associated with ~1 MHz resonance frequencies.

Although the pressure at the focus will be within regulatory limits, the pressure near the element surface of the optimal 1/7 configuration will exceed it. The generated pressure would fall rapidly further along the axial dimen-

TABLE III. REMAINING SNR CALCULATED USING THE MIXED/INTERLEAVED TOPOLOGIES.

f_0 [MHz]	Pitch	Number of receivers	Fundamental SNR	2nd Harmonic SNR	3rd Harmonic SNR	4th Harmonic SNR	5th Harmonic SNR
1.2	1/2	44	74	63	52	42	32
	1/3	59	23	56	55	45	35
	1/4	66	15	41	56	46	36
	1/5	70	13	36	50	46	36
	1/6	73	11	32	46	46	37
	1/7	75	9	30	42	47	37
	1/8	77	8	27	37	47	37

sion, because of the small size of the elements in the lateral dimension. Therefore, this issue could be solved by mounting a thin slab of low-loss material with an acoustic impedance close to that of tissue on the front of the transducer.
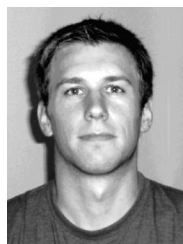
VII. Conclusion

The optimal transmit frequency for superharmonic echocardiography was found to be 1.0 to 1.2 MHz. For superharmonic abdominal imaging, this frequency was found to be 1.7 to 1.9 MHz. For 2nd-harmonic echocardiography, the optimal transmit frequency of 1.8 MHz reported in the literature was corroborated, and for 2nd-harmonic abdominal imaging, a frequency of 2.5 MHz was found.

The optimal topology for superharmonic echocardiography was the mixed transducer configuration with 1 transmit element per 6 receive elements. This configuration improves the SNR by ~5 dB compared with the interleaved (1/2) design reported in the literature [19], [37].

References

[1] M. Averkiou, D. Roundhill, and J. Powers, "A new imaging technique based on the nonlinear properties of tissues," in *Proc. IEEE Ultrasonics Symp.*, 1997, pp. 1561–1566.

[2] J. Thomas and D. Rubin, "Tissue harmonic imaging: Why does it work?" *J. Am. Soc. Echocardiogr.*, vol. 11, no. 8, pp. 803–808, 1998.

[3] V. F. Humphrey, "Nonlinear propagation in ultrasonic fields: Measurements modelling and harmonic imaging," *Ultrasonics*, vol. 38, no. 1-8, pp. 267–272, 2000.

[4] R. Shapiro, J. Wagreich, R. Parsons, A. Stancato-Pasik, H.-C. Yeh, and R. Lao, "Tissue harmonic imaging sonography: Evaluation of image quality compared with conventional sonography," *Am. J. Roentgenol.*, vol. 171, no. 5, pp. 1203–1206, 1998.

[5] F. Tranquart, N. Grenier, V. Eder, and L. Pourcelot, "Clinical use of ultrasound tissue harmonic imaging," *Ultrasound Med. Biol.*, vol. 25, no. 6, pp. 889–894, 1999.

[6] B. Ward, A. Baker, and V. Humphrey, "Nonlinear propagation applied to the improvement of resolution in diagnostic medical ultrasound," *J. Acoust. Soc. Am.*, vol. 101, no. 1, pp. 143–154, 1997.

[7] A. Bouakaz and N. de Jong, "Native tissue imaging at superharmonic frequencies," *IEEE Trans. Ultrason. Ferroelectr. Freq. Control*, vol. 50, no. 5, pp. 496–506, May. 2003.

[8] S. Zhou, P. Reynolds, and J. A. Hossack, "Improving the performance of capacitive micromachined ultrasound transducers using modified membrane and support structures," in *Proc. IEEE Ultrasonic Symp.*, Rotterdam, The Netherlands, 2005, pp. 1925–1928.

[9] D. M. Mills, "Medical imaging with capacitive micromachined ultrasound transducer (cMUT) arrays," in *Proc. IEEE Ultrasonic Symp.*, Montreal, Canada, 2004, pp. 384–390.

[10] G. G. Yaralioglu, B. Bayram, and B. T. Khuri-Yakub, "Finite element analysis of CMUTs: Conventional vs. collapse operation modes," in *Proc. IEEE Ultrasonic Symp.*, Vancouver, Canada, 2006, pp. 586–589.

[11] P. W. Rehrig, W. S. Hackenberger, and X. Jiang, "Status of piezoelectric single crystal growth for medical transducer applications," in *Proc. IEEE Ultrasonic Symp.*, Honolulu, HI, 2003, pp. 766–769.

[12] M. J. Zipparo, C. G. Oakley, D. M. Mills, A. M. Dentinger, and L. S. Smith, "A multirow single crystal phased array for wideband ultrasound imaging," in *Proc. IEEE Ultrasonic Symp.*, Montreal, Cananda, 2004, pp. 1025–1029.

[13] H. Li, Y. C. Li, D. Zhou, J. Peng, H. S. Luo, and J. Y. Dai, "Application of PMNPT single crystal in a 3.2 MHz phased-array ultrasonic medical imaging transducer," in *Proc. IEEE Int. Symp. Applications of Ferroelectricity*, Nara-city, Japan, 2007, pp. 572–574.

[14] J. A. Hossack and B. A. Auld, "Improving the characteristics of a transducer using multiple piezoelectric layers," *IEEE Trans. Ultrason. Ferroelectr. Freq. Control*, vol. 40, no. 2, pp. 131–139, Mar. 1993.

[15] S. Zhou and J. A. Hossack, "Investigation of digital filtering for stacked, phased ultrasound transducers," in *Proc. IEEE Ultrasonic Symp.*, Munich, Germany, 2002, pp. 1201–1204.

[16] J. A. Hossack, P. Mauchamp, and L. Ratsimandresy, "A high bandwidth transducer optimized for harmonic imaging," in *Proc. IEEE Ultrasonic Symp.*, San Juan, Puerto Rico, 2000, pp. 1021–1024.

[17] I. Akiyama, S. Saito, and A. Ohya, "Development of an ultrabroadband ultrasonic imaging system: Prototype mechanical sector device," *J. Med. Ultrasound*, vol. 33, no. 2, pp. 71–76, Jun. 2006.

[18] G. Ferin, M. Legros, N. Felix, C. Notard, and L. Ratsimandresy, "Ultra-wide bandwidth array for new imaging modalities," in *Proc. IEEE Ultrasonic Symp.*, New York, NY, 2007, pp. 204–207.

[19] A. Bouakaz, F. J. ten Cate, and N. de Jong, "A new ultrasonic transducer for improved contrast nonlinear imaging," *Phys. Med. Biol.*, vol. 49, no. 16, pp. 3515–3525, 2004.

[20] P. van Neer, G. Matte, M. Danilouchkine, C. Prins, F. van den Adel, and N. de Jong, "Super harmonic imaging: Development of an interleaved phased array transducer," *IEEE Trans. Ultrason. Ferroelectr. Freq. Control*, vol. 57, no. 2, pp. 455–468, 2010.

[21] X. Lurton, *An Introduction to Underwater Acoustics: Principles and Applications*. Chichester, UK: Praxis Publishing Ltd, 2002.

[22] J. A. Jensen and N. B. Svendsen, "Calculation of pressure field from arbitrarily shaped, apodized and excited ultrasound transducers," *IEEE Trans. Ultrason. Ferroelectr. Freq. Control*, vol. 39, no. 2, pp. 262–267, Mar. 1992.

[23] J. A. Jensen, "Field: A program for simulating ultrasound systems," *Med. Biol. Eng. Comput.*, vol. 34, suppl. 1, pt. 1, pp. 351–353, 1996.

[24] R. S. C. Cobbold, *Foundations of Biomedical Ultrasound*. New York, NY: Oxford University Press, 2007, pp. 227–251 and 437–438.

[25] J. Huijssen and M. D. Verweij, "A filtered convolution method for the computation of acoustic wave fields in a very large spatiotemporal domains," *J. Acoust. Soc. Am.*, vol. 125, no. 4, pp. 1868–1878, 2009.

[26] J. Huijssen and M. D. Verweij, "An iterative method for the computation of non-linear, wide angle, pulsed acoustic fields of medical diagnostic transducers," *J. Acoust. Soc. Am.*, vol. 127, no. 1, pp. 33–44, 2010.

[27] Y. S. Lee and M. F. Hamilton, "Time domain modeling of pulsed finite-amplitude sound beams," *J. Acoust. Soc. Am.*, vol. 97, no. 2, pp. 906–917, 1995.

[28] M. Hamilton and D. Blackstock, *Non Linear Acoustics.* San Diego, CA: Academic Press, 1998

[29] T. S. Hart and M. F. Hamilton, "Nonlinear effects in focused sound beams," *J. Acoust. Soc. Am.*, vol. 84, no. 4, pp. 1488–1496, 1988.

[30] P. L. M. J. van Neer, G. Matte, J. Sijl, J. M. G. Borsboom, and N. de Jong, "Transfer functions of US transducers for harmonic imaging and bubble responses," *Ultrasonics*, vol. 46, no. 4, pp. 336–340, 2007.

[31] F. A. Duck, *Physical Properties of Tissues.* San Diego, CA: Academic Press, 1990, pp. 80–139.

[32] J. N. Tjotta, S. Tjotta, and E. H. Vefring, "Effects of focusing on the nonlinear-interaction between 2 collinear finite-amplitude sound beams," *J. Acoust. Soc. Am.*, vol. 89, no. 3, pp. 1017–1027, 1991.

[33] J. N. Tjotta, S. Tjotta, and E. H. Vefring, "Propagation and interaction of 2 collinear finite-amplitude sound beams," *J. Acoust. Soc. Am.*, vol. 88, no. 6, pp. 2859–2870, 1990.

[34] J. Huijssen, "Modeling of nonlinear medical diagnostic ultrasound," Ph.D. dissertation, Laboratory of Electromagnetic Research, Delft University of Technology, Delft, The Netherlands, 2008.

[35] G. Matte, J. Borsboom, P. L. M. J. van Neer, and N. de Jong, "Estimating acoustic peak pressure generated by ultrasound transducers from harmonic distortion level measurement," *Ultrasound Med. Biol.*, vol. 34, no. 9, pp. 1528–1532, 2008.

[36] J. Kasprzak, B. Paelinck, F. Ten Cate, W. Vletter, N. De Jong, D. Poldermans, A. Elhendy, A. Bouakaz, and J. R. Roelandt, "Comparison of native and contrast-enhanced harmonic echocardiography for visualization of left ventricular endocardial border," *Am. J. Cardiol.*, vol. 83, no. 2, pp. 211–217, 1999.

[37] P. L. M. J. van Neer, G. M. Matte, M. G. Danilouchkine, C. Prins, F. van den Adel, and N. de Jong, "Super-harmonic imaging: development of an interleaved phased-array transducer," *IEEE Trans. Ultrason. Ferroelectr. Freq. Control*, vol. 57, no. 2, pp. 455–468, 2010.

Mikhail G. Danilouchkine was born in Ivanovo, in the former USSR, in 1969. He earned the M.Sc. degree (summa cum laude) in applied physics and mathematics from Moscow Institute for Physics and Technology, Moscow, Russia, in 1992. His Ph.D. study was successfully completed in the field of biophysics and bioelectromagnetism of the human heart from the same establishment in 1995. From 1995 through 1997, he was enrolled at the post-master program at Eindhoven University of Technology, Eindhoven, The Netherlands, and was awarded a Professional Doctorate in Engineering in computer science. Since 2005 he has been affiliated with the Dept. of Biomedical Engineering, Thoraxcentre, Erasmus Medical Center, Rotterdam, The Netherlands. His interests include signal and image processing, knowledge guided segmentation and registration of medical images, visualization of scientific data, and tissue elasticity imaging.

Jacobus Huijssen received the B.Sc. and the M.Sc. degrees in electrical engineering from Delft University of Technology, Delft, The Netherlands, in 2000 and 2003, respectively. In 2003, he joined the Laboratory of Electromagnetic Research at the same university, where he obtained his Ph.D. degree in 2008 in the modeling of nonlinear ultrasound fields to assist in the development of medical phased array transducers optimized for harmonic imaging. He was shortlisted for the 2009 Dutch Simon Stevin Gezel award for innovative Ph.D. research. In 2009, he joined the Noise and Vibration research group of the Faculty of Engineering Sciences at the Catholic University of Leuven, Leuven, Belgium, where he held a position as postdoctoral research fellow on simulation methods for structural vibroacoustic and electromagnetic field problems. In 2010, he was awarded a research mandate scholarship from the Flemish Science and Technology Foundation for the integration of linear and nonlinear piezoelectric device models in vibroacoustic field simulation methods, in which he operates in close cooperation with LMS International, a world-leading company in vibroacoustic simulation software.

Jacobus Huijssen's research interests incorporate computational models for linear and nonlinear acoustics, vibroacoustics, piezoelectrics and electromagnetics, with applications to medical ultrasound imaging, underwater sound, and aerospace and automotive industrial problems.

Guillaume Matte graduated from the University of Aix-Marseille III, Marseille, France. He received his Master's degree in biomedical engineering in 2005 from the Ecole Supérieure d'Ingénieurs de Luminy. That same year, he joined the department of biomedical engineering of the Thoraxcentre of Erasmus Medical Center, Rotterdam, The Netherlands. There he worked on nonlinear ultrasound for medical imaging techniques and transducer design. In 2008, he began work for IXSEA (La Ciotat, France) on electro-acoustic transducer design for underwater applications. In the meantime, he completed his Ph.D. degree from Erasmus University of Rotterdam, which he earned in 2010.

Paul L. M. J. van Neer was born in Heerlen, the Netherlands, in 1982. He earned the M.Sc. degree in biomedical technology at the Eindhoven University of Technology (Eindhoven, The Netherlands) in 2005. The same year, he worked for the Signal Processing Systems Group, Department of Electrical Engineering, Eindhoven University of Technology, on ultrasound contrast agent applications. In 2006, he joined the Department of Biomedical Engineering, Thoraxcentre, Erasmus Medical Center, Rotterdam, The Netherlands, and obtained his Ph.D. degree in the field of medical ultrasound in 2010. His current interests include transducer design, nonlinear ultrasound, tissue imaging methods, and ultrasound contrast agent imaging methods.

Martin Verweij (M'10) was born in Alphen aan den Rijn, The Netherlands, in 1961. He received his B.Eng. degree in electrical engineering from the Municipal Polytechnical School, The Hague, The Netherlands, in 1983. He received his M.Sc. degree in electrical engineering in 1988, and his Ph.D. degree in technical sciences in 1992, both from the Delft University of Technology, Delft, The Netherlands. From 1993 to 1997, he was a research fellow of the Royal Netherlands Academy of Arts and Sciences. In 1995 and 1997, he was a Visiting Scientist at Schlumberger Cambridge Research, Cambridge, England. In 1998, he became an Assistant Professor, and later that same year an Associate Professor, both in the Laboratory of Electromagnetic Research, Delft University of Technology. In this position, he is involved in researching and teaching the fundamentals of electromagnetic, acoustic, and elastodynamic fields and waves. His research focuses on the theoretical modeling and numerical simulation of acoustic waves, formerly in the application area of geophysical exploration, and since 2005, in the application area of medical ultrasound. He is the originator of the Iterative Nonlinear Contrast Source (INCS) method for the computation of nonlinear ultrasound fields. For his teaching, he was elected "Best Teacher of the Electrical Engineering Curriculum" in the academic year 2001–2002. Dr. Verweij is project leader of the Dutch Technology Foundation (STW) project on superharmonic imaging, and participates in research involving nonlinear propagation, transducer design, and excitation schemes. He is a member of IEEE and the Acoustical Society of America.

Nico de Jong graduated from the Delft University of Technology, The Netherlands, in 1978. He received his M.Sc. degree in the field of pattern recognition. Since 1980, he has been a staff member of the Thoraxcentre of the Erasmus University Medical Center, Rotterdam. In 1993, he received his Ph.D. degree for Acoustic properties of ultrasound contrast agents. Since 2003, he has been a part-time professor at the University of Twente in the group Physics of Fluids headed by Detlef Lohse (Spinoza winner, 2005). He is organizer of the annual European Symposium on Ultrasound Contrast Imaging, held in Rotterdam and attended by approximately 175 scientists from universities and industries all over the world. He is on the safety committee of WFUMB (World Federation of Ultrasound in Medicine and Biology), assiociate editor of *Ultrasound in Medicine and Biology* and has been guest edititor for special issues of different journals. Over the last 5 years, he has given more than 30 invited lectures and has given numerous scientific presentations for international industries. He teaches at Technical Universities and the Erasmus Medical Center. He has been Promotor of 13 Ph.D. students and is currently supervising 9 Ph.D. students. He has published more than 135 scientific papers and has several patents on ultrasound contrast imaging and transducer design.